WILEY-VCH

Edited by Xiao-Feng Wu

Transition Metal-Catalyzed Heterocycle Synthesis via C-H Activation

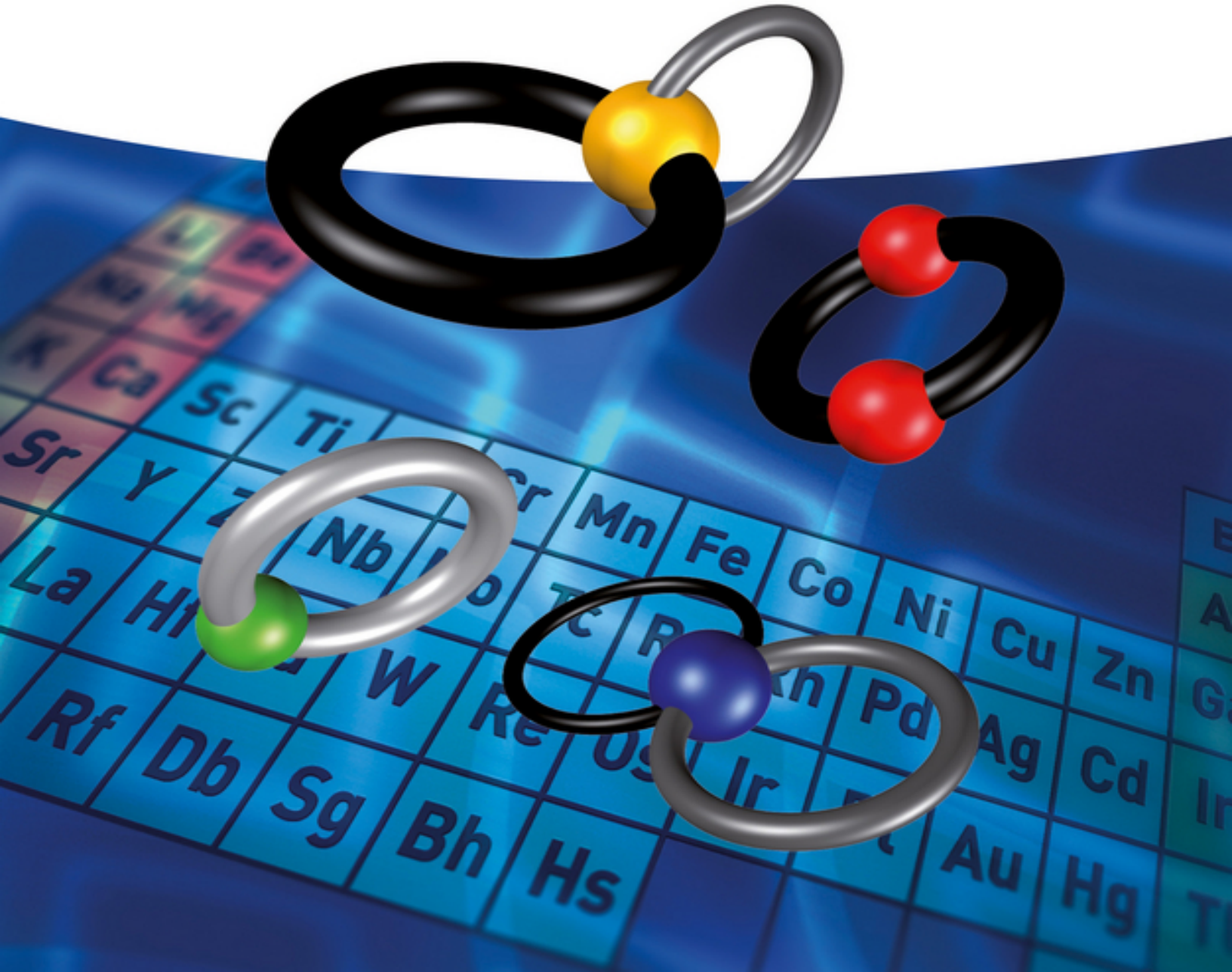

Table of Contents

List of Illustrations

Chapter 1: Computational Studies of Heteroatom-Assisted C−H Activation at Ru, Rh, Ir, and Pd as a Basis for Heterocycle Synthesis and Derivatization

Figure 1.7 *Meta* selectivity via remote CN directing groups: (a) Pd-catalyzed alkenylation of **16–17** in the presence of an MPAA coligand via computed C−H activation transition state **TS16** featuring deprotonation by the *N*-acyl group (Ar = 2-C_6H_4−CN) [22] and (b) Pd/Ag-catalyzed alkenylation of **18–19** via computed heterobimetallic C−H activation transition state **TS18** [23].

Figure 1.8 (a) Pd-catalyzed amination of N-arylbenzamides (experiment, R = ^{t}Bu, Ar = 4-$C_6F_4CF_3$, X = Cl, OAc,OBz) and (b) computed CsF-stabilized heterobimetallic transition state (R = Ar = H) [25].

Figure 1.9 Computed C−H activation transition state for C(sp^3)−H bond activation of oxazolines (R^1 = R^2 = ^{t}Bu, **25a**; R^1 = Et, R^2 = ^{i}Pr, **25b**), highlighting the preferred *anti* arrangement for **25a** [30].

Figure 1.10 Enantioselective indoline formation from *R*-**26** via Pd−NHC intermediate **27.** Free energies (at 413 K) for the enantio-determining C−H activation transition states leading to products *cis*-/*trans*-**28** and **29** are indicated in kcal mol^{-1} [31a].

Figure 1.11 Computed reaction profile for C−H activation of benzene at Pd(κ^2-CO_2H)$_2$; MP4(SDQ) energies are in kcal mol^{-1} and selected distances in Å [32].

Figure 1.12 Computed transition state for C−H bond activation of C_6F_5H at Pd(Ph)(HCO_3)(P^tBu_2Me), with selected distances in Å [33].

Figure 1.13 Computed free energy activation barriers (kcal mol^{-1}) for C−H activation of selected heterocycles at Pd(Ph)(OAc)(PMe_3) [35].

Figure 1.23 (a) Cyclometalation of *N*-alkylimines (**H-L$_{1-5}$**) and 2-phenylpyridine (**H-L$_6$**) at [MCl$_2$Cp*]$_2$ (M = Rh, Ir); relative experimental and computed reactivities for substrates **H-L$_{1-6}$** at [MCl$_2$Cp*]$_2$, (b) M = Rh, and (c) M = Ir. Computed data (kcal mol^{-1}) give the overall free energy changes, ΔG_{calc}, for M = Rh and calculated activation barriers, $\Delta G^{\ddagger}_{calc}$, for M = Ir [61].

Figure 1.24 Computed free energy reaction profiles (kcal mol^{-1}) for C−H activation of **H-L$_3$** at [MCl$_2$Cp*]$_2$ for M = Ir (in CH_2Cl_2) and M = Rh (in MeOH). Computed C−H activation transition states are shown with key distances in Å (Rh, plain text; Ir, italics) and nonparticipating H atoms omitted for clarity.

Figure 1.25 Comparison of OMe-assisted and σ-bond metathesis transition states at [Ir]R species ([Ir] = Ir(acac)$_2$; R = OMe, **TS50** [68]; R = PhCH$_2$CH$_2$, **TS51** [69]). Key selected distances are given in Å.

Figure 1.26 Key distances (Å) and relative free energies (kcal mol^{-1}) in transition states for C(sp^3)−H activation (**TS54**) and C(sp^2)−H activation (**TS55**) of an α-imidazolium ester, **53**, at Ir(OAc)$_2$Cp*.

Figure 1.27 Computed catalytic cycle for the coupling of *N*-acetoxybenzamide with acetylene at Rh(OAc)$_2$Cp [75]. Computed free energies of intermediates and transition states are given in kcal mol^{-1}, with the latter indicated in square brackets, and are quoted relative to the reactants at 0.0 kcal mol^{-1}.

Figure 1.28 (a) Reactions of PhC(O)NH(OR) (OR = OMe, OPiv) with ethene at Rh(OAc)$_2$Cp* [76]. Key

the N−H-activated form of **I.** [b]The formation of **II** from **I** involves several steps and **TS(I–II)** is the highest point in this process.

Figure 1.34 Rate-limiting transition states with key distances (Å) for the C−H activation of 5-methyl-3-phenylpyrazole at {Rh(OAc)Cp*} (**TS(I–II)$_{Rh}$**) and {Ru(OAc)(*p*-cymene)} (**TS(I–II)$_{Ru}$**). Associated experimental and computed k_H/k_D KIE data are also shown [84].

Figure 1.35 (a) Ru-catalyzed oxidative coupling of benzylamines with 2-butyne to form isoquinolones; (b) transition state for C−H activation via external deprotonation with key distances (Å); and (c) key stationary points on the free energy profile (kcal mol^{-1}; energies quoted relative to the reactants at 0.0 kcal mol^{-1}). Double arrows indicate several steps are involved, with the energy of the highest transition state between the two minima indicated in square brackets [85].

Figure 1.36 (a) Ir-catalyzed isocoumarin formation [86] and (b) Rh-catalyzed phosphaisocoumarin formation [87].

Figure 1.37 (a) Rh-catalyzed alkenylation of *m*-tolyldimethylcarbamate with ethyl acrylate and (b) key stationary points on the free energy profile (kcal mol^{-1}; energies quoted relative to the reactants at 0.0 kcal mol^{-1}) [90].

Figure 1.38 Rh-catalyzed alkenylation reactions: (a) 3-phenylpyrazole with $H_2C{=}CHR$ (R = Ph, CO_2Me) [92] and (b) *N*-methoxybenzamide with dimethyl-2-vinylcyclopropane-1,1-dicarboxylate [93].

tetrahydroazepin
tetrahydrobenz[*b*]azepin-4-ones
tetrahydrofuran
tetrahydrooxepin
tetrahydroquinolines
tetramethylaminopyridyl radical (TEMPO)
texaline
1,2,3-triazoles
thiazoles
    annuloline and siphonazole
    JNK3 inhibitors
    texaline, febuxostat and muscoride
    tyrosine kinase inhibitor
thiophenes
2-thiophenyl derivative
thiophenoazepinones
three-phase tests
tipifarnib
triarylphosphines
1,2,3-triazoles
tricyclic furan
tricyclic indole
tricyclic pyrroles
tricyclic sultone
tricyclic thiophene